The Astrophysical Journal Letters, 867:L22 (5pp), 2018 November 10 https://doi.org/10.3847/2041-8213/aaeb34

Experimental Testing of Scattering Polarization Models

W. Li[1], R. Casini[1], S. Tomczyk[1], E. Landi Degl'Innocenti[2,4], and B. Marsell[3]
[1] High Altitude Observatory, National Center for Atmospheric Research,[5] P.O. Box 3000, Boulder, CO 80307-3000, USA; wenxianli10@yahoo.com
[2] Dip. di Astronomia e Scienza dello Spazio, Università di Firenze, L.go E. Fermi 2, I-50125 Firenze, Italy
[3] Stetson University, 421 North Woodland Boulevard, DeLand, FL 32723, USA
Received 2018 September 12; revised 2018 October 19; accepted 2018 October 24; published 2018 November 5

Abstract

We realized a laboratory experiment to study the scattering polarization of the Na I D-doublet at 589.0 and 589.6 nm in the presence of a magnetic field. This work was stimulated by solar observations of that doublet, which have proven particularly challenging to explain through available models of polarized line formation, even to the point of casting doubts on our very understanding of the underlying physics. The purpose of the experiment was to test a quantum theory for the polarized scattering of spectrally flat incident radiation, on which much of the current magnetic diagnostics of stellar atmospheres is based. The experiment has confirmed the predictions of that theory, and its adequacy for the modeling of scattering polarization under flat-spectrum illumination.

Key words: magnetic fields – polarization – scattering

1. Introduction

Over the past few decades, scattering polarization and its modification in the presence of a magnetic field have become fundamental diagnostics of many physical properties of astrophysical plasmas (Trujillo Bueno 2001b; Casini & Landi Degl'Innocenti 2008). In particular, spectrally resolved observations of the polarized radiation from the solar disk near the limb, using high-sensitivity ($S/N \gtrsim 10^3$) instrumentation, have produced an extremely rich amount of data (the so-called "Second Solar Spectrum;" Stenflo & Keller 1997; Gandorfer 2000) of great diagnostic value (Landi Degl'Innocenti 1997; Stenflo et al. 1998; Manso Sainz & Trujillo Bueno 2003; Trujillo Bueno et al. 2004). However, the interpretation of these observations has often proven to be difficult, and continues to challenge our understanding of how polarized radiation is produced and transported in the solar atmosphere.

One notable example is the linear polarization of the D_1 resonance line of neutral sodium at 589.6 nm, which has been the target of many observations (Stenflo & Keller 1996; Stenflo et al. 2000; Trujillo Bueno 2001a; Bommier & Molodij 2002). In the optically thin limit, this $J = 1/2 \leftrightarrow J' = 1/2$ transition cannot produce broadband linear polarization, despite the polarizability of its hyperfine-structure (HFS) levels (Mitchell & Zemansky 2009; Casini et al. 2002; Trujillo Bueno et al. 2002). This is because the spectral shape of its emissivity turns out to be anti-symmetric, and so it averages out to zero when the transition is spectrally unresolved. However, observations by Stenflo & Keller (1996) and Stenflo et al. (2000) surprisingly had shown the presence of a strong linear polarization signal in the line core, raising many questions about its origin, and even about the reliability of those observations (Trujillo Bueno 2001a; Bommier & Molodij 2002). While the complexity of the line-formation problem in the optically thick and magnetized atmosphere of the Sun is expected to play a role in determining the spectral shape of this line, the "enigma" posed by those observations has even brought some authors (Thalmann et al. 2006; Stenflo 2015) to question the adequacy of the quantum-electrodynamic formalism on which many of our interpretation tools for solar polarimetric observations are based (Landi Degl'Innocenti & Landolfi 2004). This impasse convinced us of the need to put this theoretical framework to the test with a specifically designed laboratory experiment.

2. Experiment

2.1. Experimental Setup

We built a scattering experiment where a vapor of neutral sodium under controlled conditions of temperature and magnetic field is illuminated by a light beam. The scattered radiation is analyzed polarimetrically, separately for the $D_1(3p^2P_{1/2} \rightarrow 3s^2S_{1/2}$, 589.6 nm) and $D_2(3p^2P_{3/2} \rightarrow 3s^2S_{1/2}$, 589.0 nm) transitions.

A top-view schematics of the experiment is shown in Figure 1. This consists of a Na I vapor cell surrounded by two air-cooled Helmholtz-coil pairs, and flanked by four "legs" with different functions. Light enters the apparatus from the bottom leg, is focalized at the center of the vapor cell, and the light scattered from the vapor at 90° is analyzed in the left leg. The top leg uses a photodiode to monitor the light level of the source, and the right leg is used to input specific polarization states for the purpose of polarimetric calibration.

The center of the sodium cell is located at the intersection of the four legs of the apparatus. The sodium is evaporated into the cell from a reservoir that is temperature controlled at a typical value of 205 °C. Along with the sodium vapor, the cell also contains 17 mmHg of Ar buffer gas. The two Helmholtz-coil pairs allow the generation of a magnetic field between 0 and 150 G with any desired direction in the scattering plane (plane of Figure 1).

To ensure the condition of *complete frequency redistribution* (CRD; see Modeling section) of the scattered radiation, we employed a 50 W halogen bulb with stabilized output, which provides a largely flat and structureless spectrum over the frequency range of the D lines. An input polarization selector, consisting of a linear polarizer mounted in a precision rotation

[4] Egidio Landi Degl'Innocenti was one of the promoters of the experiment, and a principal contributor to its interpretation and to the drafting of this Letter. Sadly, he passed away, prematurely and unexpectedly, before he could see its completion.
[5] The National Center for Atmospheric Research is sponsored by the National Science Foundation.

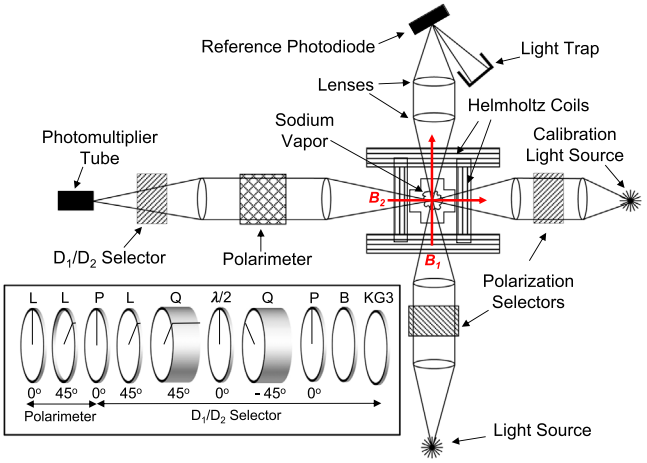

Figure 1. Top-view diagram of the experimental setup. The four "legs" of the experiment are (clockwise from the bottom): input beam, scattered light analysis, light-level monitor, and calibration. The inset shows the elements of the polarimeter and D_1/D_2 selector (L = LCVR, P = polarizer, Q = quartz plate, $\lambda/2$ = half-waveplate, B = 9.5 nm blocker).

stage and a fixed $\lambda/4$ retarder, can be placed in the beam following the light source, allowing an arbitrary polarization state to be input to the vapor. In this Letter, we only present data and modeling for the case of unpolarized input.

The analysis leg consists of a Stokes polarimeter, a filter that selects the D line to be observed, and a photomultiplier tube (PMT) with a gain of approximately 2×10^6. Details of the polarimeter and D_1/D_2 selector are shown in the inset diagram of Figure 1. The polarimeter consists of two Nematic Liquid Crystal Variable Retarders (LCVRs) followed by a linear polarizer. The LCVRs are oriented with their fast axes at 0° and 45°, with the linear polarizer also oriented at 0°. The orientation of this polarizer sets the reference direction of positive Stokes Q, which is approximately normal to the scattering plane. This system allows the analysis of the complete polarization state of the scattered light by measuring its intensity at selected retardations of the two LCVRs.

The D_1/D_2 line selector consists of a birefringent crystal between polarizers (Mascart 1874), producing a channel spectrum with a free spectral range equal to twice the separation of the D-doublet (1.195 nm). In order to minimize the shift of the bandpass with inclination angle through the selector, we have used quartz crystals in a wide-fielded configuration (Lyot 1944; Evans 1948). The channel spectrum is shifted by a third Nematic LCVR with its fast axis aligned with that of the first crystal, which allows the electro-optical selection of either of the D lines. For simplicity, the analyzing polarizer of the polarimeter serves also as the entrance linear polarizer of the D_1/D_2 selector. To limit the number of unwanted orders of the D_1/D_2 selector we additionally employ a 9.5 nm wide interference filter centered at 590.5 nm (blocker), and a Schott KG3 filter. To compensate for thermal shifts of the D_1/D_2 selector, we monitor its temperature and adjust the LCVR voltage to achieve the proper tuning.

The calibration leg contains a light source and input polarization selector that is identical to those in the input-beam leg. For the purpose of polarimetric calibration, light is input from the calibration leg into the analysis leg in the absence of sodium vapor (cold cell) and magnetic field. By measuring the output signal for known input polarization states, we can compute the response matrix of the polarimeter, which maps the measured Stokes vectors to the true ones.

2.2. Measurements

We measured the scattering polarization of the D lines in the presence of a magnetic field in the scattering plane, with strength between 0 and 150 G in steps of 10 G, and inclination from the direction of the incident radiation between 0° and 90° (respectively, $\boldsymbol{B}_1$ and $\boldsymbol{B}_2$ in Figure 1) in steps of 30°. The calibration data were obtained before and after the scattering measurements. A measurement of the background signal was taken at the beginning of the experiment with the cold cell and no magnetic field. This background is a combination of Rayleigh scattering of the incident radiation by the Ar buffer gas, and parasitic reflections off the cell walls that make it into the analysis leg.

A computer running LabVIEW performs all experiment controls and data logging functions. The voltage output of the PMT is digitized with 16-bit precision. Each measurement consists of an average of 10^4 samples taken over 250 ms followed by a 125 ms delay to allow for LCVR relaxation. A Stokes vector measurement is obtained by measuring the intensity coarsely corresponding to the six modulated states $I \pm (Q, U, V)$, and making the proper combinations and polarization cross-talk corrections to obtain I, Q, U, V. This is accomplished by multiplying the measured Stokes vector by the polarimeter response matrix to obtain the true Stokes vector. The elements of the resulting Stokes vector have a typical uncertainty of $\sim 10^{-3}$.

3. Modeling

To model the scattering polarization from the Na I vapor we rely on several physical assumptions.

(1) The flat spectrum of the light source implies that radiation scattering can be described as the incoherent succession of single-photon absorption and re-emission (CRD hypothesis; Heitler 1954; Sakurai 1967; Landi Degl'Innocenti & Landolfi 2004).

(2) Isotropic elastic collisions with the Ar buffer gas contribute to the statistical equilibrium of the Na I atoms, leading to a partial depolarization of the atomic levels. The corresponding two depolarizing rates (respectively, for the orientation and the alignment of the atomic levels) are free parameters of the model. For simplicity, we adopt the same rates for the ground and excited states. However, the ensuing depolarization is nearly total for the ground state because of its much longer lifetime. These collisions also contribute to the realization of the CRD conditions of line formation in our experiment.

(3) In order to fit the data, we found necessary to add a small collisional de-excitation rate to the statistical equilibrium of the Na I atoms. A possible explanation is that the collisions with the Ar buffer gas may not be perfectly elastic. However, the low temperature of the sodium vapor implies that collisional excitation from the ground state is negligible. Thus the observed line intensity is dominated by the resonance scattering of the incident radiation, without any measurable contribution from Planckian radiation at the vapor temperature.

Additionally, collisional transfer between the $P_{1/2}$ and $P_{3/2}$ levels can be important, as the energy separation

is about 10^3 times smaller than the excitation potential of the D-doublet. These transfer collisions predominantly produce a depolarization of the levels (Kerkeni 2002; Kerkeni & Bommier 2002), adding to the effect of elastic collisions already considered. Because the relative contribution between transfer and elastic collisions to this depolarization is not constrained by our data, we chose to simply ignore transfer collisions in our model.

(4) The gas cell is operated at a regime around unit optical depth. Hence, differential saturation of the line components must be taken into account (Leroy 1962; Calamai et al. 1975). Additionally, polarization effects due to quantum interference between the fine-structure levels of the atom cannot in principle be ruled out under our experimental conditions. All of these effects can confidently be modeled assuming that the fraction of the vapor contributing to the scattered radiation has spatially homogeneous thermodynamic and magnetic properties.

The differential saturation of the magnetic components of the lines (Leroy 1962; Calamai et al. 1975) turns out to be essential for the interpretation of the experimental results. In contrast, for the particular thermal and magnetic regimes of the experiment, our modeling shows that quantum interference between the $P_{1/2}$ and $P_{3/2}$ levels brings a much smaller, yet measurable, correction to the polarization.

(5) Magnetic-induced dichroism affects the transfer of both the sodium emission and the background radiation through the optically thick vapor. Hence, the background measurements cannot in general be subtracted from the experimental data, in order to isolate the contribution of the D lines to the observed polarization. For this reason, we treat the background radiation as a boundary term in the solution of the radiative transfer equation for the Stokes vector $\boldsymbol{S} \equiv (I, Q, U, V)$,

$$\frac{d}{ds}\boldsymbol{S} = -\boldsymbol{K}\,\boldsymbol{S} + \varepsilon. \tag{1}$$

where s is the coordinate along the optical path, ε is the polarized emissivity vector (source term), and $\boldsymbol{K}$ is the 4×4 absorption matrix, which also accounts for dichroism and magneto-optical effects (Landi Degl'Innocenti & Landolfi 2004). The experimental data must then be compared with the numerical solution of Equation (1) in a spatially homogeneous medium (Landi Degl'Innocenti & Landolfi 2004, Section 8.3), taking into account the background term, and after convolution with the transmission profile of the D_1/D_2 selector.

The above hypotheses suggest that we adopt the formalism of the *multi-term* atom with HFS (Casini & Manso Sainz 2005; Belluzzi et al. 2015) to model the scattering polarization by the magnetized sodium vapor, as this takes into account the effects of quantum interference between the $P_{1/2}$ and $P_{3/2}$ levels. However, it is instructive to look at the algebraic formulation of the *multi-level* atom with HFS given by Landi Degl'Innocenti & Landolfi (2004), because it allows us to better grasp how the free parameters of the model and the magnetic field affect the scattering polarization in each of the two D lines.

The broadband polarized emissivity due to radiation scattering in a two-level atom (J_ℓ, J_u) with HFS is (see Landi Degl'Innocenti & Landolfi 2004, Section 10.22)

$$\bar{\varepsilon}_i(\boldsymbol{\Omega}) = k_{\rm L}^{\rm A} \oint \frac{{\rm d}\boldsymbol{\Omega}'}{4\pi} \sum_{j=0}^{3} P_{ij}(\boldsymbol{\Omega}, \boldsymbol{\Omega}'; \boldsymbol{B})_{\rm hfs}\, S_j(\boldsymbol{\Omega}'), \tag{2}$$

where $P_{ij}(\boldsymbol{\Omega}, \boldsymbol{\Omega}'; \boldsymbol{B})_{\rm hfs}$ is the *Hanle phase matrix*, and $i, j = 0, 1, 2, 3$, enumerates the four Stokes parameters I, Q, U, V. The interpretation of Equation (2) is straightforward: the Stokes parameter $S_j(\boldsymbol{\Omega}')$ of the incident radiation along the direction $\boldsymbol{\Omega}'$ is scattered into the direction $\boldsymbol{\Omega}$ and polarization state i, with a frequency integrated cross-section given by the line absorption coefficient, $k_{\rm L}^{\rm A}$. We recall that the incident radiation in our experiment has no spectral structure around the transition frequency of the line. Evidently, the assumption of a spectrally flat incident radiation is necessary in order to write Equation (2).

The Hanle phase matrix is given by

$$P_{ij}(\boldsymbol{\Omega}, \boldsymbol{\Omega}'; \boldsymbol{B})_{\rm hfs} = \sum_{KK'Q} (-1)^Q\, \mathcal{T}^K_Q(i, \boldsymbol{\Omega})\mathcal{T}^{K'}_{-Q}(j, \boldsymbol{\Omega}') \times W_{KK'Q}(J_\ell, J_u; \boldsymbol{B})_{\rm hfs}, \tag{3}$$

where the polarization tensors $T^K_Q(i, \boldsymbol{\Omega})$, with $K = 0, 1, 2$ and $Q = -K, \ldots, K$, characterize the scattering geometry, and are tabulated in Landi Degl'Innocenti & Landolfi (2004). The *line polarizability factor* $W_{KK'Q}(J_\ell, J_u; \boldsymbol{B})_{\rm hfs}$ describes the magnetic dependence of the Hanle phase matrix. When stimulated emission and the polarization of the J_ℓ level can both be neglected, like in the case of our experiment, the polarizability factor can be expressed in algebraic form (see Landi Degl'Innocenti & Landolfi 2004, Equation (10.167)):

$$\begin{aligned} W_{KK'Q}(J_\ell, J_u; \boldsymbol{B})_{\rm hfs} &= \frac{3(2J_u+1)}{2I+1} \begin{Bmatrix} 1 & 1 & K \\ J_u & J_u & J_\ell \end{Bmatrix} \begin{Bmatrix} 1 & 1 & K' \\ J_u & J_u & J_\ell \end{Bmatrix} \\ &\times \sum_{F_u F'_u F''_u F'''_u} \sqrt{(2K+1)(2K'+1)(2F_u+1)(2F'_u+1)(2F''_u+1)(2F'''_u+1)} \begin{Bmatrix} J_u & J_u & K \\ F_u & F'_u & I \end{Bmatrix} \begin{Bmatrix} J_u & J_u & K' \\ F''_u & F'''_u & I \end{Bmatrix} \\ &\times \sum_{f_u f'_u} \sum_{ij} C^i_{F_u}(J_u f_u) C^i_{F''_u}(J_u f_u) C^j_{F'_u}(J_u f'_u) C^j_{F'''_u}(J_u f'_u) \begin{pmatrix} F_u & F'_u & K \\ -f_u & f'_u & -Q \end{pmatrix} \begin{pmatrix} F''_u & F'''_u & K' \\ -f_u & f'_u & -Q \end{pmatrix} \\ &\times \{1 + \delta^{(K)}_{J_u} + \epsilon_{J_u J_\ell} + {\rm i}[\omega_j(J_u f'_u) - \omega_i(J_u f_u)]\big/A_{J_u J_\ell}\}^{-1}. \end{aligned} \tag{4}$$

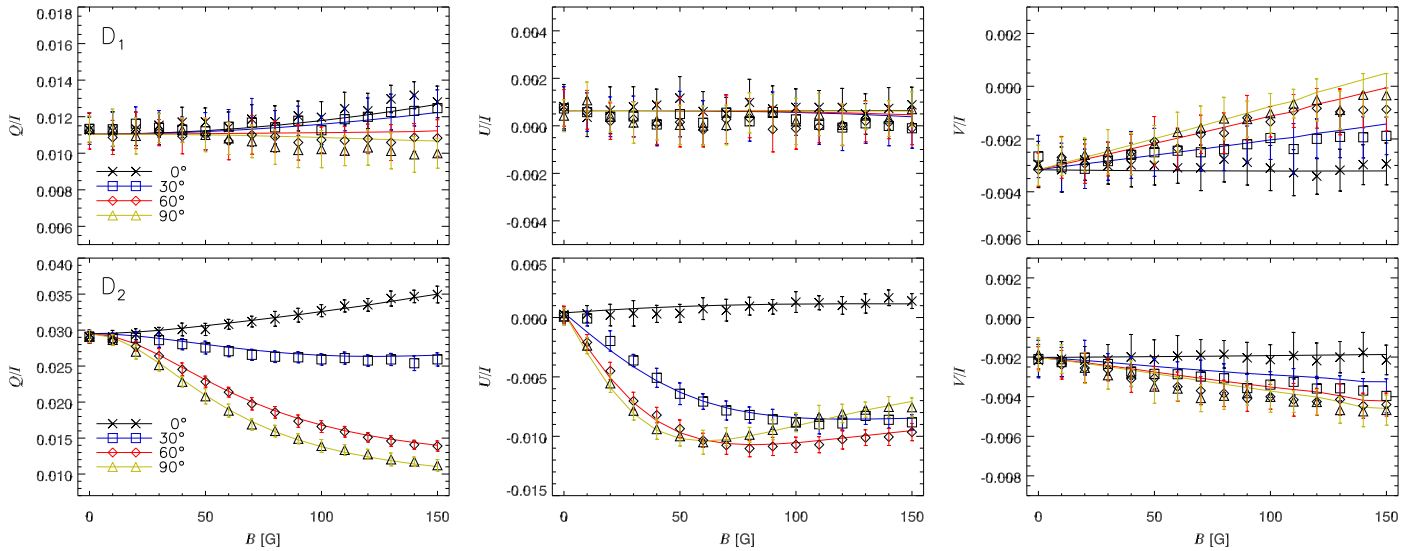

Figure 2. Broadband fractional polarization Q/I, U/I, and V/I (left to right) of the D_1 (top) and D_2 (bottom) lines as a function of magnetic field strength, for various geometries of the applied magnetic field. The measurements are represented by different symbols (with error bars) and colors, for different values of ϑ_B. The continuous curves of matching color represent the model.

The coefficients $C^i_{F_u}(J_u f_u)$, with $F_u = |J_u - I|, \ldots, J_u + I$, are the components of the ith eigenvector of the HFS subspace of J_u with magnetic quantum number f_u, and $\omega_i(J_u f_u)$ is the corresponding eigenvalue. They are determined via diagonalization of the magnetic Hamiltonian, assuming the direction of $\boldsymbol{B}$ as the quantization axis. In the denominator of Equation (4), the imaginary term accounts for polarization effects associated with the energy differences between the atomic eigenstates (Hanle effect, HFS depolarization, level-crossing interference). $\delta^{(K)}_{J_u}$ and $\epsilon_{J_u J_\ell}$ are, respectively, the depolarizing and inelastic collision rates, expressed in units of the Einstein coefficient $A_{J_u J_\ell} \approx 6.2 \times 10^8\ \mathrm{s}^{-1}$ (see Landi Degl'Innocenti & Landolfi 2004, Equation (10.54)). For the contribution of the level population to the emissivity ($K = 0$), $\delta^{(0)}_{J_u} = 0$, thus the polarizability factor only contains the free parameters $\delta^{(1)}_{J_u}$ (orientation relaxation), $\delta^{(2)}_{J_u}$ (alignment relaxation), and $\epsilon_{J_u J_\ell}$ (collisional de-excitation).

For the multi-level atom, a distinct set of these three free parameters must be specified for each of the two D lines. In the multi-term formalism, instead, we only need the three parameters $\delta^{(1,2)} \equiv \delta^{(1,2)}_{L_u}$ and $\epsilon \equiv \epsilon_{L_u L_\ell}$, expressed in units of the D-doublet spontaneous rate $A_{L_u L_\ell} \approx 6.2 \times 10^8\ \mathrm{s}^{-1}$, where $L_u = 1$ and $L_\ell = 0$. On the other hand, for the multi-term atom, an algebraic expression of the broadband emissivity analogous to Equations (2)–(4) cannot be attained *separately* for each line of the doublet.

4. Results

Figure 2 reports one set of measurements (resulting from the average of 12 different realizations of the experiment) of the broadband fractional polarization of the two D lines (symbols with error bars). In Figure 2, the continuous curves represent the fit of the experimental data provided by the model described in the previous section. It is important to remark that the zero-field values in all plots, except for the Q/I polarization of D_2, are dominated by the transfer of the background polarization through the optically thick vapor. In the absence of background radiation, those values would be zero (within the polarimetric accuracy of the experiment). The intensity and polarization of the background are measured at the beginning of the experiment (cold cell). The ratio $I_{\mathrm{bkg}}/(I_{\mathrm{line}} + I_{\mathrm{bkg}})$ turns out to be about 17% for D1 and 12% for D2, while the polarization of the background is very consistent between the two spectral ranges, with $(Q_{\mathrm{bkg}}, U_{\mathrm{bkg}}, V_{\mathrm{bkg}})/I_{\mathrm{bkg}} \simeq (1, 0.064, 0.004, -0.018)$.

Numerical modeling based on Equations (2)–(4) predicts that all states of polarization of D_1, as well as the V/I polarization of D_2 should remain largely insensitive to the magnetic field in an optically thin vapor, well below the 10^{-3} sensitivity level of our experiment. The large departures from such ideal behavior observed in the experimental data, especially for the V/I polarization, are mainly due to the differential saturation of the magnetic components of the lines as they are transferred through the optically thick vapor (Leroy 1962; Calamai et al. 1975). In order to fit the measurements, we determined an optical depth $\tau_{D_2} \approx 1.3$. The non-flat behavior of the U/I polarization of D_2 for $\vartheta_B = 0°$ is explained by a small error of the apparatus in setting the desired magnetic field inclination, which we modeled with a $-2°$ offset from the nominal values of ϑ_B.

The remaining free parameters of the model are the depolarizing collision rates $\delta^{(1,2)}$ and the de-excitation collision rate ϵ. The value of $\delta^{(2)}$ strongly affects the linear polarization amplitudes of D_2, and characteristically the location of the two crossing points among the U/I polarization curves for $\vartheta_B \neq 0$. We used these constraints to determine a value $\delta^{(2)} \approx 19$. The $\delta^{(1)}$ rate affects instead the V/I polarization caused by the presence of atomic orientation. In the case of unpolarized input, this contribution is rapidly suppressed by depolarizing collisions. Thus, the value of $\delta^{(1)}$ is only weakly constrained by the data shown in Figure 2. However, when the incident light is circularly polarized, the observed V/I signals are much larger (by a factor $\sim$10, in the case of D_2) than those shown in Figure 2. Using such measurements (not reported here), we could determine $\delta^{(1)} \approx 13$. Finally, by matching the zero-field value of the Q/I polarization of D_2, after taking into account the depolarization produced by $\delta^{(2)}$, we estimated $\epsilon \approx 0.44$.

5. Conclusions

The agreement between theory and experiment shown in Figure 2 is remarkable, considering that the fitting of the reported data (384 independent polarization measurements) practically relies on only three model parameters, τ, $\delta^{(2)}$, and ϵ. This demonstrates that the quantum-electrodynamic formalism on which our model of scattering polarization in the CRD limit is based (Landi Degl'Innocenti & Landolfi 2004) is completely adequate when the incident radiation is spectrally flat over the wavelength range of the atomic transition.

The Na I D lines, however, are among the strongest absorption features of the solar spectrum, and the flat-spectrum approximation breaks down in the solar atmosphere, especially with regard to the treatment of the quantum interference between the $P_{1/2}$ and $P_{3/2}$ levels. Therefore, new polarization effects due to the partial redistribution of the radiation frequency (PRD) can be expected for these lines (Belluzzi & Trujillo Bueno 2013; Belluzzi et al. 2015). Recent work (Landi Degl'Innocenti et al. 1996; Bommier 1997, 2017; Casini et al. 2014, 2017) has formally extended the theory of Landi Degl'Innocenti & Landolfi (2004) beyond the CRD limit, in order to model PRD effects in radiation scattering. Indeed, when these effects are taken into account in the modeling of the polarized D_1 line (Belluzzi & Trujillo Bueno 2013; Belluzzi et al. 2015), even its finer spectral details as observed on the Sun (Trujillo Bueno 2001a; Bommier & Molodij 2002) can be reproduced.

The successful interpretation of our experiment provides compelling evidence of the fundamental validity of the quantum-electrodynamic formalism used to interpret the many polarization phenomena routinely observed on the Sun and in other astrophysical objects. At the same time, together with the recent modeling by Belluzzi & Trujillo Bueno (2013) and Belluzzi et al. (2015), our results strongly support the conclusion that the peculiarities of the observed polarization of the D_1 line (Stenflo & Keller 1996; Stenflo et al. 2000; Trujillo Bueno 2001a; Bommier & Molodij 2002) must be traced back to the complexity of the line formation problem in realistic atmospheric scenarios, or in extreme cases to possible instrumental effects that must be identified and corrected for.

Financial support for this experiment was provided by the National Center for Atmospheric Research through the Director's Opportunity Funds. We thank G. Card for his contribution to the design and construction of the experiment. The authors have benefited from many discussions with several colleagues, who at times have also assisted in various aspects of the experiment. In particular, we thank A. de Wijn, R. Manso Sainz, A. López Ariste, and J. O. Stenflo. We thank J. Trujillo Bueno for helpful comments and suggestions on the final version of the manuscript. We thank the anonymous referee for critical questions that helped clarify the presentation of these results.

ORCID iDs

R. Casini https://orcid.org/0000-0001-6990-513X
S. Tomczyk https://orcid.org/0000-0001-7399-3013

References

Belluzzi, L., Landi Degl'Innocenti, E., & Trujillo Bueno, J. 2015, ApJ, 812, 73
Belluzzi, L., & Trujillo Bueno, J. 2013, ApJ, 774, 28
Belluzzi, L., Trujillo Bueno, J., & Landi Degl'Innocenti, E. 2015, ApJ, 814, 116
Bommier, V. 1997, A&A, 328, 726
Bommier, V. 2017, A&A, 607, 50
Bommier, V., & Molodij, G. 2002, A&A, 381, 241
Calamai, G., Landi Degl'Innocenti, E., & Landi Degl'Innocenti, M. 1975, A&A, 45, 297
Casini, R., del Pino Alemán, T., & Manso Sainz, R. 2017, ApJ, 848, 99
Casini, R., & Landi Degl'Innocenti, E. 2008, in Plasma Polarization Spectroscopy, ed. T. Fujimoto & A. Iwamae (Berlin: Springer), 247
Casini, R., Landi Degl'Innocenti, E., Landolfi, M., & Trujillo Bueno, J. 2002, ApJ, 573, 864
Casini, R., Landi Degl'Innocenti, M., Manso Sainz, R., Landi Degl'Innocenti, E., & Landolfi, M. 2014, ApJ, 791, 94
Casini, R., & Manso Sainz, R. 2005, ApJ, 624, 1025
Evans, J. W. 1948, JOSA, 38, 1083
Gandorfer, A. 2000, The Second Solar Spectrum: A High Spectral Resolution Polarimetric Survey of Scattering Polarization at the Solar Limb in Graphical Representation, Vol. I: 4625 Å to 6995 Å (Zürich: VDF Hochschulverlag)
Heitler, W. 1954, Quantum Theory of Radiation (3rd ed.; Oxford: Oxford Univ. Press)
Kerkeni, B. 2002, A&A, 390, 783
Kerkeni, B., & Bommier, V. 2002, A&A, 394, 707
Landi Degl'Innocenti, E. 1997, Natur, 392, 256
Landi Degl'Innocenti, E., Landi Degl'Innocenti, M., & Landolfi, M. 1996, in Forum THéMIS, ed. N. Mein & S. Sahal-Bréchot (Paris: Observatoire de Paris), 59
Landi Degl'Innocenti, E., & Landolfi, M. 2004, Polarization in Spectral Lines (Dordrecht: Kluwer)
Leroy, J.-L. 1962, AnAp, 25, 127
Lyot, B. 1944, AnAp, 7, 31
Manso Sainz, R., & Trujillo Bueno, J. 2003, PhRvL, 91, 111102
Mascart, M. 1874, Ann. Sci. Éc. Norm. Supér, 3, 363
Mitchell, A. C. G., & Zemansky, M. W. 2009, Resonance Radiation and Excited Atoms (Cambridge: Cambridge Univ. Press)
Sakurai, J. J. 1967, Advanced Quantum Mechanics (Boston: Addison-Wesley)
Stenflo, J. O. 2015, ApJ, 801, 70
Stenflo, J. O., Gandorfer, A., & Keller, C. U. 2000, A&A, 355, 781
Stenflo, J. O., & Keller, C. U. 1996, Natur, 382, 588
Stenflo, J. O., & Keller, C. U. 1997, A&A, 321, 927
Stenflo, J. O., Keller, C. U., & Gandorfer, A. 1998, A&A, 329, 319
Thalmann, C., Stenflo, J. O., Feller, A., & Cacciani, A. 2006, in ASP Conf. Ser. 358, Solar Polarization 4, ed. R. Casini & B. W. Lites (San Francisco, CA: ASP), 323
Trujillo Bueno, J. 2001a, in ASP Conf. Ser. 236, Advanced Solar Polarimetry —Theory, Observation, and Instrumentation, ed. M. Sigwarth (San Francisco, CA: ASP), 141
Trujillo Bueno, J. 2001b, in ASP Conf. Ser. 236, Advanced Solar Polarimetry —Theory, Observation, and Instrumentation, ed. M. Sigwarth (San Francisco, CA: ASP), 161
Trujillo Bueno, J., Casini, R., Landolfi, M., & Landi Degl'Innocenti, E. 2002, ApJ, 566, 53
Trujillo Bueno, J., Shchukina, N., & Asensio Ramos, A. 2004, Natur, 430, 326